Inorg. Chem. **2006**, *45*, 4047–4054

Unusual Mn–Mn Spin Coupling in the Polar Intermetallic Compounds $CaMn_2Sb_2$ and $SrMn_2Sb_2$

Svilen Bobev* and Justin Merz

Department of Chemistry, University of Delaware, Newark, Delaware 19716

Ana Lima, Veronika Fritsch, Joe D. Thompson, and John L. Sarrao

Los Alamos National Laboratory, Los Alamos, New Mexico 87545

Michael Gillessen and Richard Dronskowski

Institut für Anorganische Chemie, Rheinisch-Westfälische Technische Hochschule, Landoltweg 1, 52056 Aachen, Germany

Received January 17, 2006

Large single-crystals of two polar intermetallic phases, $CaMn_2Sb_2$ and $SrMn_2Sb_2$, have been grown using In or Sn as metal fluxes and characterized by single-crystal X-ray diffraction. The two compounds are isostructural and crystallize with the $CaAl_2Si_2$ structure (space group $P\bar{3}m1$, No. 164) with unit cell parameters determined at 120(2) K of $a = 4.5204(6)$ Å, $c = 7.456(2)$ Å and $a = 4.5802(17)$ Å, $c = 7.730(5)$ Å for $CaMn_2Sb_2$ and $SrMn_2Sb_2$, respectively. Temperature- and field-dependent dc- and ac-magnetization measurements suggest complex magnetic ordering of the Mn moments below ca. 250 and 35 K for $CaMn_2Sb_2$ and below ca. 265 K for $SrMn_2Sb_2$. Resistivity measurements reveal metallic-like temperature dependence with $\rho_{290} = 40$ mΩ cm for $CaMn_2Sb_2$ and $\rho_{290} = 100$ mΩ cm for $SrMn_2Sb_2$ with negligible magnetoresistance at 5 K in applied magnetic fields up to 10 kOe. Spin-polarized DFT electronic structure calculations confirm the metallic-like properties and provide further evidence for a magnetic structure where Mn atoms form two magnetic sublattices with ferromagnetic coupling within them and strong antiferromagnetic coupling between them.

Introduction

Several general types of compounds have been extensively studied in recent years, notably manganese oxides, because of their scientific and technological importance as "giant" or "colossal" magnetoresistive (GMR or CMR) materials.[1−5] Whereas magnetoresistance in metallic thin films can be appreciable,[1] changes in the resistivity as a function of the external magnetic field in bulk metals are typically negligible.[6] Nevertheless, there have been several reports on intermetallic phases that exhibit GMR or CMR at moderate magnetic fields.[5] Among these, Mn-containing Zintl compounds from the $A_{14}MnPn_{11}$ family (A = alkaline-earth or divalent rare-earth metals; Pn = pnicogens (i.e., P, As, Sb, Bi)) are the most prevalent, and their crystal chemistry and physical properties have been extensively studied.[5] The importance of the Mn-centered tetrahedral units to the magnetism and the conductivity of the "14−1−11" series has been well-documented and understood, and these dis-

* To whom correspondence should be addressed. Phone: (302) 831-8720. Fax: (302) 831-6335. E-mail: sbobev@chem.udel.edu.

(1) Baibich, M. N.; Broto, J. M.; Fert, A.; Nguyen van Dan, F.; Petroff, F.; Etienne, P.; Crenzert, G.; Friedrich, A.; Chazelas, J. *Phys. Rev. Lett.* **1988**, *61*, 1979.
(2) Hellman, F.; Tran, M. Q.; Gebala, A. E.; Wicox, E. M.; Dynes, R. C. *Phys. Rev. Lett.* **1996**, *77*, 4652.
(3) (a) Rao, C. N. R.; Cheetham, A. K. *Science* **1996**, *272*, 369. (b) Subramanian, M. A.; Toby, B. H.; Ramirez, A. P.; Marshall, W. J.; Sleight, A. W.; Kwei, G. H. *Science* **1996**, *273*, 81.
(4) Ramirez, A. P.; Cava, R. J.; Krajewski, J. *Nature* **1997**, *386*, 156.
(5) (a) Chan, J. Y.; Kauzlarich, S. M.; Klavins, P.; Shelton, R. N.; Webb, D. J. *Phys. Rev.* **1998**, *57*, R8103. (b) Kim, H.; Klavins, P.; Kauzlarich, S. M. *Chem. Mater.* **2002**, *14*, 2308. (c) Payne, A. C.; Olmstead, M. M.; Kauzlarich, S. M.; Webb, D. J. *Chem. Mater.* **2001**, *13*, 1398. (d) Kim, H.; Olmstead, M. M.; Klavins, P.; Webb, D. J.; Kauzlarich, S. M. *Chem. Mater.* **2002**, *14*, 3382. (e) Jiang, J.; Olmstead, M. M.; Kauzlarich, S. M.; Lee, H. O.; Klavins, P.; Fisk, Z. *Inorg. Chem.* **2005**, *44*, 5322.
(6) Sechovsky, V.; Havela, L.; Prokes, K.; Nakotte, H.; de Boer, F. R.; Brück, E. *J. Appl. Phys.* **1994**, *76*, 6913.

10.1021/ic060092e CCC: $33.50
Published on Web 04/15/2006

coveries have motivated many further studies. Until now, these efforts have proven successful, and several new polar intermetallics based on condensed $MnPn_4$ building blocks have been reported, including $Ca_{21}Mn_4Sb_{18}$,[7] $Eu_{10}Mn_6Sb_{13}$,[8] Sr_2MnSb_2,[9] $EuMn_2P_2$,[10] and $YbMn_2Sb_2$,[11] to name just a few. All these compounds exhibit unusual physical properties because of direct Mn−Mn interactions, the competition and interplay of RE−Mn and RE−RE exchange interactions (RE = Eu, Yb), or both. Very recently, much experimental and theoretical attention has been focused on other types of intermetallics with unusual Mn−Mn interactions, the so-called half-metallic ferromagnets, such as some filled skutterudites, AMn_4Sb_{12},[12] half-Heusler-type phases, AMnSb,[13] and $Ga_{1-x}Mn_xPn$ III−V semiconductors,[14] which are characterized by the presence of an energy gap for the minority-spin electrons at the Fermi level.

Intrigued by the rich phenomenology of these structurally related phases, we undertook systematic studies in the corresponding Ca−Mn−Sb and Sr−Mn−Sb systems. This work aimed primarily at synthesizing $A_9Mn_{4+x}Sb_9$, isostructural with $Ca_9Zn_{4+x}Sb_9$ ($x \approx 0.5$),[15] and examination of their physical properties. The structure of the elusive compounds $Ca_9Mn_{4+x}Sb_9$ and $Sr_9Mn_{4+x}Sb_9$ could be viewed as being built of four Mn-centered Sb_4-tetrahedra, which are interconnected via corner sharing to form one-dimensional chains, which could result in unprecedented magnetic interactions. It was anticipated that by employing metals with low melting points, such as Sn or In for instance, the target materials can be synthesized as large crystals and in high yields. Instead, the flux reactions produced large crystals of $CaMn_2Sb_2$ and $SrMn_2Sb_2$ ($CaAl_2Si_2$-type),[16] the layered structures of which consist of edge-shared $MnSb_4$ tetrahedra. Although $CaMn_2Sb_2$ and $SrMn_2Sb_2$ are not new compounds,[17] their properties have never been studied. Herein, we report low-temperature single-crystal X-ray diffraction studies, temperature- and field-dependent dc and ac magnetization, field and temperature-dependent electrical resistivity, and spin-polarized band-structure calculations for the compounds $CaMn_2Sb_2$ and $SrMn_2Sb_2$.

Experimental Section

Synthesis. Large single crystals of $CaMn_2Sb_2$ (up to 5−6 mm^3) were initially identified from a reaction loaded as $Ca_9Mn_{4.5}Sb_9$ with a large excess of In or Sn metals to serve as fluxes. This reaction was intended to produce crystals of the hitherto unknown phase $Ca_9Mn_{4+x}Sb_9$, isostructural with $Ca_9Zn_{4+x}Sb_9$ and $Yb_9Zn_{4+x}Sb_9$.[15] Subsequently, once the structure and the composition of the product were established, crystals of $CaMn_2Sb_2$ (and later of $SrMn_2Sb_2$) were grown successfully from Sn flux reactions, loaded with the proper stoichiometric ratios of Ca/Mn/Sb = 1:2:2. The alumina crucibles proved suitable for these experiments and there were no signs of unwanted side reactions.

All manipulations were performed in an argon-filled glovebox. The starting materials, Ca, Sr, Mn, Sb, and In or Sn (all from Alfa, purity greater than 99.9%), were used as received and were loaded in alumina crucibles. The crucibles were then placed in fused silica ampules, which were in turn closed under vacuum by flame sealing. The reaction mixtures were heated in a programmable muffle furnace at 1273 K for 48 h, followed by a slow cooling (−10°/hour) to 773 K. At that point, the molten flux was removed by centrifugation. Comprehensive details on the flux-growth synthetic procedures can be found elsewhere.[18] On-stoichiometry reactions were carried out as well, but the reaction outcomes of those always contained side products, $Ca_{11}Sb_{10}$ ($Sr_{11}Sb_{10}$) or $Ca_{14}MnSb_{11}$ ($Sr_{14}MnSb_{11}$) and $Mn_{1-x}Sb$.[16] Attempts to synthesize isostructural $REMn_2Sb_2$ compounds (RE = trivalent rare-earth) from analogous stoichiometric or flux reactions were unsuccessful.

Single-Crystal X-ray Diffraction. Dark crystals with a silver-metallic luster of both $CaMn_2Sb_2$ and $SrMn_2Sb_2$ were selected from Sn flux reactions. The irregularly shaped crystals were cut to the desired dimensions and were then mounted on glass fibers. Routine data collections were carried out using a Bruker SMART CCD diffractometer (monochromatized Mo Kα radiation) equipped with a low-temperature apparatus and operated at 120(2) K. Data acquisitions were performed using SMART[19] in four batch runs at ϕ = 0, 90, 180, and 270° (450 frames each). The frame width was 0.4° θ in ω with 10 s exposure time per frame. A total of 718 reflections were collected for a crystal of $CaMn_2Sb_2$ with dimensions of 0.05 × 0.05 × 0.02 mm (T_{min}/T_{max} = 0.514/0.730, 131 unique reflections, R_{int} = 0.017) up to a diffraction angle, $2\theta_{max}$, of ≈52°; a total of 1005 reflections were collected for a crystal of $SrMn_2Sb_2$ with dimensions of 0.04 × 0.03 × 0.02 mm (T_{min}/T_{max} = 0.425/0.628, 136 unique reflections, R_{int} = 0.034) up to a diffraction angle, $2\theta_{max}$, of ≈53°. The data were corrected for Lorentz and polarization effects and integrated using the SAINT software.[20] Semiempirical absorption corrections were applied with the aid of SADABS.[21] The structures were refined on F^2 using the SHELXTL, version 6.12, package.[22] Details of the data collection

(7) Holm, A.; Olmstead, M. M.; Kauzlarich, S. M. *Inorg. Chem.* **2003**, *42*, 1973.
(8) Holm, A. P.; Park, S. M.; Condron, C. L.; Olmstead, M. M.; Kim, H.; Klavins, P.; Grandjean, F.; Hermann, R. P.; Long, G. J.; Kanatzidis, M. G.; Kauzlarich, S. M.; Kim, S. J. *Inorg. Chem.* **2003**, *42*, 4660.
(9) Park, S. M.; Kim, S. J.; Kanatzidis, M. G. *Inorg. Chem.* **2005**, *44*, 4979.
(10) Payne, A. C.; Sprauve, A. E.; Olmstead, M. M.; Kauzlarich, S. M.; Chan, J. Y.; Reisner, B. A.; Lynn, J. W. *J. Solid State Chem.* **2002**, *163*, 498.
(11) (a) Nirmala, R.; Morozkin, A. V.; Suresh, K. G.; Kim, H.-D.; Kim, J.-Y.; Park, B.-G.; Oh, S.-J.; Malik, S. K. *J. Appl. Phys.* **2005**, *97*, 10M511. (b) Rühl, R.; Jeitschko, W. *Mater. Res. Bull.* **1979**, *14*, 513.
(12) de Groot, R. A.; Mueller, F. M.; van Engen, P. G.; Buschow, K. H. J. *Phys. Rev. Lett.* **1983**, *50*, 2024.
(13) Sales, B. C. In *Handbook on the Chemistry and Physics of the Rare Earths*; Gschneidner, K. A., Jr., Eyring, L., Eds.; Elsevier: Amsterdam, 2003; Vol. 33, p 1.
(14) (a) Dietl, T.; Ohno, O.; Matsukura, F.; Cibert, J.; Ferrand, D. *Science* **2000**, *287*, 1019. (b) Litvinov, V. I.; Dugaev, V. K. *Phys. Rev. Lett.* **2001**, *86*, 5593.
(15) (a) Bobev, S.; Thompson, J. D.; Sarrao, J. L.; Olmstead, M. M.; Hope, H.; Kauzlarich, S. M. *Inorg. Chem.* **2004**, *43*, 5044. (b) Kim, S.-J.; Salvador, J.; Bilc, D.; Mahanti, S. D.; Kanatzidis, M. G. *J. Am. Chem. Soc.* **2001**, *123*, 12704. (c) Brechtel, E.; Cordier, G.; Schäfer, H. *Z. Naturforsch.* **1979**, *34B*, 1229. (d) Brechtel, E.; Cordier, G.; Schäfer, H. *Z. Naturforsch.* **1981**, *36B*, 1099.
(16) *Pearson's Handbook of Crystallographic Data for Intermetallic Phases*; Villars, P., Calvert, L. D., Eds.; ASM International: Materials Park, OH, 1991.
(17) Cordier, G.; Schäfer, H. *Z. Naturforsch.* **1976**, *31B*, 1459.
(18) (a) Canfield, P. C.; Fisk Z. *Philos. Mag. B* **1992**, *65*, 1117. (b) Kanatzidis, M. G.; Pöttgen, R.; Jeitschko, W. *Angew. Chem., Int. Ed.* **2005**, *44*, 6996.
(19) *SMART NT*, version 5.63; Bruker Analytical X-ray Systems, Inc.: Madison, WI, 2003.
(20) *SAINT NT*, version 6.45; Bruker Analytical X-ray Systems, Inc.: Madison, WI, 2003.
(21) *SADABS NT*, version 2.10; Bruker Analytical X-ray Systems, Inc.: Madison, WI, 2001.
(22) *SHELXTL*, version 6.12; Bruker Analytical X-ray Systems, Inc.: Madison, WI, 2001.

Table 1. Selected Crystallographic Data for $CaMn_2Sb_2$ and $SrMn_2Sb_2$

chemical formula	$CaMn_2Sb_2$	$SrMn_2Sb_2$
fw	393.46	441.00
space group, Z	$P\bar{3}m1$ (No. 164), 1	
unit cell parameters (Å)	$a = 4.5204(6)$	$a = 4.5802(17)$
	$c = 7.456(2)$	$c = 7.730(5)$
	$V = 131.94(4)$ Å^3	$V = 140.44(12)$ Å^3
radiation, λ (Å)	Mo Kα, 0.71073	
temp (K)	120(2)	
ρ_{calc} (g/cm^3)	4.952	5.214
μ (cm^{-1})	155.90	231.27
final R1[a]/wR2[b] ($I > 2\sigma_I$)	0.0198/0.0448	0.0239/0.0480
final R1[a]/wR2[b] (all data)	0.0222/0.0456	0.0302/0.0508

[a] $R1 = \sum||F_o| - |F_c||/\sum|F_o|$. [b] $wR2 = [\sum[w(F_o^2 - F_c^2)^2]/\sum[w(F_o^2)^2]]^{1/2}$; $w = 1/[\sigma^2F_o^2 + (AP)^2 + BP]$, $P = (F_o^2 + 2F_c^2)/3$; A and B are weight coefficients.

Table 2. Atomic Coordinates and Equivalent Isotropic Displacement Parameters (U_{eq})[a] for $CaMn_2Sb_2$ and $SrMn_2Sb_2$

atom	site	x	y	z	U_{eq} (Å^2)
			$CaMn_2Sb_2$		
Ca	1*a*	0	0	0	0.0089(7)
Mn	2*d*	1/3	2/3	0.6216(2)	0.0085(5)
Sb	2*d*	1/3	2/3	0.2513(1)	0.0070(3)
			$SrMn_2Sb_2$		
Sr	1*a*	0	0	0	0.0096(5)
Mn	2*d*	1/3	2/3	0.6194(3)	0.0098(6)
Sb	2*d*	1/3	2/3	0.2625(1)	0.0087(4)

[a] U_{eq} is defined as 1/3 of the trace of the orthogonalized U_{ij} tensor.

Table 3. Important Bond Distances (Å) in $CaMn_2Sb_2$ and $SrMn_2Sb_2$

$CaMn_2Sb_2$			$SrMn_2Sb_2$		
Sb−	Mn	2.761(2)	Sb−	Mn	2.759(3)
	3 × Mn	2.7765(7)		3 × Mn	2.798(1)
	3 × Ca	3.2128(6)		3 × Sr	3.333(1)
Mn−	Sb	2.761(2)	Mn−	Sb	2.759(3)
	3 × Sb	2.7765(7)		3 × Sb	2.798(1)
	3 × Mn	3.178(2)		3 × Mn	3.225(3)
	3 × Ca	3.843(1)		3 × Sr	3.956(2)
Ca−	6 × Sb	3.2128(6)	Sr−	6 × Sb	3.333(1)
	6 × Mn	3.843(1)		6 × Mn	3.956(2)

and structure refinements for all three crystals are given in Table 1; positional and equivalent isotropic displacement parameters and important bond distances are listed in Tables 2 and 3, respectively. Further information in the form of a combined CIF is available as Supporting Information.

Property Measurements. Property measurements were performed on single crystals of $CaMn_2Sb_2$ and $SrMn_2Sb_2$ grown in Sn flux. Crystals from different reaction batches were measured to ensure the reproducibility of the results reported herein.

Magnetic Susceptibility Measurements. Routine dc-magnetization measurements (both field and zero-field cooling) were performed in a Quantum Design MPMS SQUID magnetometer from 2 to 350 K in magnetic fields of 500−1000 Oe. The samples, with a typical mass of approximately 15−20 mg, were loaded in plastic straws and secured within pieces of quartz wool. The raw data were corrected for the holder's diamagnetic contribution and converted to molar susceptibility.

The real and imaginary components of the ac susceptibility were measured from 2 to 300 K in the frequency interval of 1−10 kHz in a Quantum Design PPMS system up to fields of 50 kOe. Further pulsed-field measurements were taken at the National High Magnetic Field Laboratory (NHMFL) at Los Alamos National Laboratory, in the temperature interval from 0.6 to 100 K and up to magnetic fields of 450 kOe. Oriented ($H \parallel c$ axis), large single crystals of $CaMn_2Sb_2$ were used in these experiments.

Resistivity Measurements. The electrical resistivity measurements were carried out on a Quantum Design PPMS system using a four-probe technique from 5 to 300 K. For each measurement, polished single crystals were used, and the direction of the current was presumed to be within the *ab* plane. Resistance as a function of temperature in an applied field of 10 kOe was measured on crystals of $CaMn_2Sb_2$ only.

Theoretical Methodology. Electronic structure calculations on $CaMn_2Sb_2$ were performed using the linear muffin-tin orbital (LMTO) method[23−25] in its tight-binding representation,[26] which corresponds to a fast linearized form of the Korringa−Kohn−Rostoker (KKR) method.[27,28] The calculations were carried out using the TB-LMTO-ASA program with a scalar-relativistic Hamiltonian and the atomic-spheres approximation.[29] Electronic energies and magnetic moments were calculated via density-functional theory (DFT) based on the local-density approximation (LDA) for the exchange-correlation functional as parametrized by von Barth and Hedin[30] or based on the parametrization by Vosko, Wilk, and Nusair[31] augmented with gradient corrections[32] to follow the generalized-gradient approximation (GGA).

The chemical bonding was investigated using the crystal orbital Hamilton population (COHP) analysis,[33] which is an energy-resolved partitioning technique of the band-structure energy (sum of the Kohn−Sham eigenvalues) in terms of atomic and bonding contributions.[34] All electronic structure calculations were carried out using nonspin-polarized (nonmagnetic) and spin-polarized (ferromagnetic and antiferromagnetic) approaches, with a total of 756 and 1500 k points in the irreducible Brillouin zones of the crystallographic unit cell (nonmagnetic/ferromagnetic case) and of the antiferromagnetic supercell, respectively. In the latter case, the symmetry of the system was lowered to obtain a model in which the Mn planes could be treated separately.

Results and Discussion

Structure. A number of intermetallic compounds with the $CaAl_2Si_2$ structure (an ordered derivative of the $CaIn_2$ type) are known,[16] and the structure and bonding in these systems have been given full consideration in several earlier publications.[35,36] Therefore, this discussion will be focused on a few specific details of the structure refinements of $CaMn_2Sb_2$ and $SrMn_2Sb_2$ at 120 K, such as the lack of structural phase transition, the changes of the interatomic distances and bond

(23) Andersen, O. K. *Phys. Rev. B* **1975**, *12*, 3060.
(24) Skriver, H. *The LMTO Method*; Springer-Verlag: Berlin, 1984.
(25) Andersen, O. K. In *The Electronic Structure of Complex Systems*; Phariseau, P.: Temmerman, M., Eds.; Plenum: New York, 1984.
(26) Andersen, O. K.; Jepsen, O. *Phys. Rev. Lett.* **1984**, *53*, 2571.
(27) Korringa, J. *Physica* **1947**, *13*, 392.
(28) Kohn, W.; Rostoker, N.; *Phys. Rev.* **1954**, *94*, 1111.
(29) Krier, G.; Jepsen, O.; Burkhardt, A.; Andersen, O. K. *The TB-LMTO-ASA program*, version 4.7; Max-Planck-Institut für Festkörperforschung: Stuttgart, Germany.
(30) von Barth, U.; Hedin, L. *J. Phys. C* **1972**, *5*, 1629.
(31) Vosko, S. H.; Wilk, L.; Nusair, M. *Can. J. Phys.* **1980**, *58*, 1200.
(32) Perdew, J. P.; Chevary, J. A.; Vosko, S. H.; Jackson, K. A.; Pederson, M. R.; Fiolhais, C. *Phys Rev. B* **1992**, *46*, 6671.
(33) Dronskowski, R.; Blöchl, P. E. *J. Phys. Chem.* **1993**, *97*, 8617.
(34) Dronskowski, R. *Computational Chemistry of Solid State Materials*; Wiley-VCH: Weinheim, New York, 2005.
(35) (a) Brock, S. L.; Greedan, J. E.; Kauzlarich, S. M. *J. Solid State Chem.* **1994**, *109*, 416. (b) Brock, S. L.; Greedan, J. E.; Kauzlarich, S. M. *J. Solid State Chem.* **1994**, *113*, 303.
(36) (a) Zheng, C.; Hoffmann, R.; Nesper, R.; von Schnering, H. G. *J. Am. Chem. Soc.* **1986**, *108*, 1876. (b) Zheng, C.; Hoffmann, R. *J. Solid State Chem.* **1988**, *72*, 58. (c) Burdett, J. K.; Miller, G. J. *Chem. Mater.* **1990**, *2*, 12.

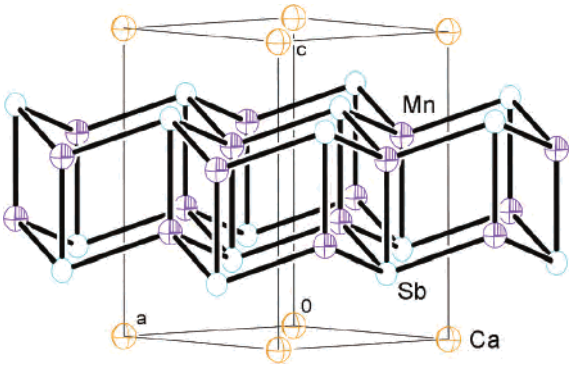

Figure 1. Trigonal structure of $CaMn_2Sb_2$, viewed approximately down the [110] direction (unit cell outlined). Thermal ellipsoids are drawn at the 98% probability level.

angles compared to those at room temperature, and the relationship of these changes to the properties the title compounds exhibit.

Figure 1 shows a perspective view of the layered trigonal crystal structure of $CaMn_2Sb_2$ and $SrMn_2Sb_2$, which can be readily described as double corrugated layers of $Mn_2Sb_2^{2-}$, separated by Ca^{2+} or Sr^{2+} cations. The two-dimensional polyanionic network may be derived either from the imaginary splitting of a wurtzite-type lattice and a subsequent reconstruction or, alternatively, from puckering of "dimerized" graphite-like layers.[36] The corresponding Sb−Mn distances fall in the narrow range from 2.761(2) to 2.7765(7) Å in $CaMn_2Sb_2$ and from 2.759(3) to 2.798(1) Å in $SrMn_2Sb_2$ (Table 3). These compare well with the sum of the covalent radii for Sb and Mn,[37] as well as with the Sb−Mn distances in other polar intermetallics such as $A_{14}MnSb_{11}$,[5] $A_{21}Mn_4Sb_{18}$ (A = Ca, Sr),[7] $Eu_{10}Mn_6Sb_{13}$,[8] Sr_2MnSb_2,[9] and $YbMn_2Sb_2$.[11] A prominent structural feature is the Sb−Mn contacts parallel to the direction of the *c* axis (referred to as "handle" bonds in earlier publications[36]), which are systematically shorter than the Sb−Mn contacts in the *ab* plane (referred to as "rib" bonds). Detailed theoretical analyses on the semiempirical level have shown that the vertical handle bond should be almost equal or shorter than the rib bonds only when the transition metal has half-filled d bands, and our experimental results are in agreement with the theory in that regard. However, it needs to be pointed that the bond length difference (Δ) between the handle and rib bonds in both $CaMn_2Sb_2$ and $SrMn_2Sb_2$ increase at low temperature: for $CaMn_2Sb_2$, $\Delta(120\ K) = -0.0155$ Å and $\Delta(293\ K) = +0.002$ Å. These changes are also reflected in the bond angles: the Sb−Mn−Sb angle at 120 K is 109.95(3)° compared to 109.71° at room temperature, whereas the complimentary Mn−Sb−Sb angle decreases at 120 K to 70.05(3)° from 70.29° at room temperature. For $SrMn_2Sb_2$ the differences are even more pronounced, $\Delta(120\ K) = -0.039$ Å and $\Delta(293\ K) = +0.028$ Å, which may suggest further stabilization of the Sb−Mn handle bonds through stronger magnetic coupling between the Mn centers at lower temperatures. These changes transpire in the distortion of the $MnSb_4$ tetrahedra: the Sb−Mn−Sb angle at 120 K is 109.05(5)° compared to 108.85° at room temperature and the corresponding Mn−Sb−Sb angle decreases to 70.95(5)° at 120 K from 71.15° at room temperature.

Specifics of the local bonding, site preferences, and differences in the bonding geometry of Mn and Sb have been discussed already.[36] It has been suggested that the more electropositive element, Mn in our case (Pauling's electronegativity 1.5),[37] should reside at the more dispersive site (i.e., the site with shorter contacts between the equivalents).[36a] It is easy to see from the selected viewing projection in Figure 1 that this position is the center of the distorted Sb_4 tetrahedron. Indeed, the corresponding Mn−Mn distances are 3.178(2) and 3.225(3) Å (Table 2) for $CaMn_2Sb_2$ and $SrMn_2Sb_2$, respectively. The Mn−Mn distances within a single Mn layer are almost 50% longer: 4.5204(6) and 4.5802(15) Å for $CaMn_2Sb_2$ and $SrMn_2Sb_2$, respectively. These contacts are much longer than the longest Mn−Mn distances in elemental α-Mn (2.885(2) Å),[16] yet they represent atomic interactions, which contribute to the overall bonding picture and the magnetic properties (below). The more electronegative Sb (Pauling's electronegativity 1.9)[37] can, in its place, be viewed as centering the umbrella-shaped Mn_4 unit ("inverted" tetrahedron).[36] These site preferences can be deduced not only from analysis of the corresponding orbitals,[36a] but also from simple geometric considerations: there will be stronger electrostatic interactions between the very electropositive Ca atoms and the nearer electronegative Sb atoms than with the Mn atoms (Figure 1), which will lead to a more significant Madelung energy contribution to the total crystal energy.

Last, the electron count in $CaMn_2Sb_2$ and $SrMn_2Sb_2$ is straightforward and can be rationalized using the classic Zintl formalism[38] in the following way: the very electropositive and divalent Ca and Sr donate their valence electrons to the electronegative Mn and Sb, which in turn form anionic substructure (the puckered $Mn_2Sb_2^{2-}$ layers). Hence, for all ions to be with closed-shell configurations, the system will require exactly 16 valence electrons. Such an electron count can obviously be achieved for d^5 and d^{10} transition metals only (e.g., Mn^{2+} and Zn^{2+}), and indeed, almost all members of the $CaAl_2Si_2$ obey these rules.[11,16,35,36] There are, however, examples such as $LnAl_2Si_2$ (Ln = trivalent rare-earth) with 17 electrons, which are therefore metallic conductors.[39] $CaMn_2Sb_2$ and $SrMn_2Sb_2$ *also* exhibit metallic-like, albeit relatively poor conductivity (below), despite formally being saltlike Zintl phases. This shortcoming can be explained if one recalls that Zintl reasoning is just a basic approach toward complicated structures, and the arguments of closed-shell configurations are greatly oversimplified. Out of the context of this approach and the Hückel theory, the metallic properties can be understood as a consequence of significant contribution of the Mn d-bands to the overall bonding, which

(37) Pauling, L. *The Nature of the Chemical Bond*; Cornell University Press: Ithaca, NY, 1960.

(38) (a) Zintl, E. *Angew. Chem.* **1939**, *52*, 1. (b) *Chemistry, Structure, and Bonding of Zintl Phases and Ions*; Kauzlarich, S. M., Ed.; VCH Publishers: New York, 1996.

(39) Kranenberg, C.; Johrendt, D.; Mewis, A.; Pöttgen, R.; Kotzyba, G.; Rosenhahn, C.; Mosel, B. D. *Solid State Sciences* **2000**, *2*, 215.

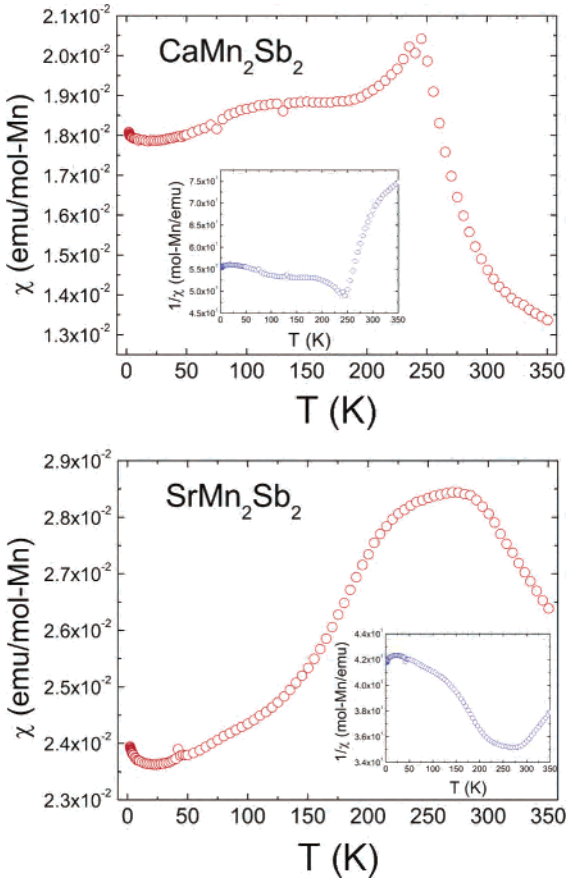

Figure 2. Temperature dependence of the dc susceptibility for polycrystalline $CaMn_2Sb_2$ and $SrMn_2Sb_2$ measured at applied field of 1 kOe. The insets show the inverse susceptibility as a function of the temperature.

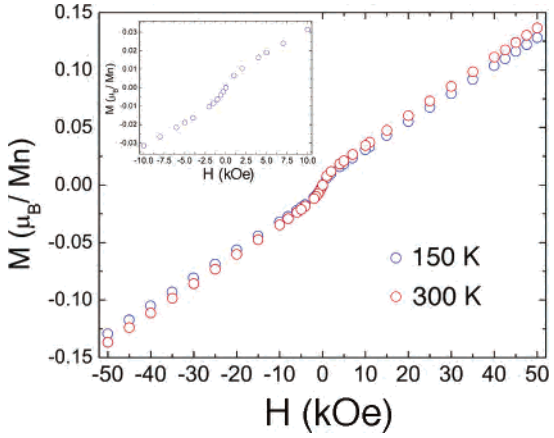

Figure 3. Field dependence of the dc susceptibility for polycrystalline $CaMn_2Sb_2$ at temperatures of 150 and 300 K (inset shows a magnified view at lower fields).

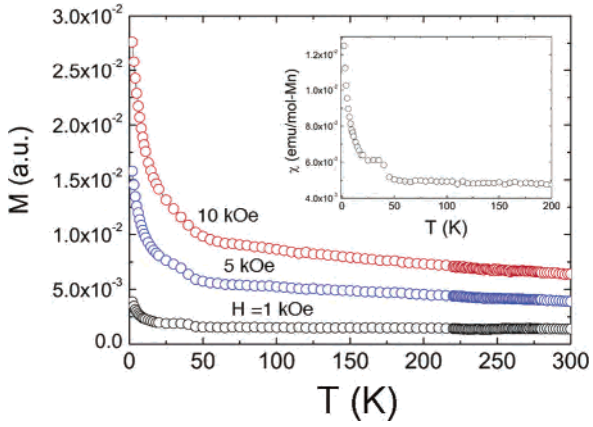

Figure 4. Temperature dependence of the ac magnetization of oriented single crystals of $CaMn_2Sb_2$ at applied fields of 1 kOe, 5 kOe, and 10 kOe. Inset shows ac susceptibility vs T at an applied field of $H = 1$ kOe.

results in metallic behavior not associated with delocalized "extra" electrons, elaborated further in the discussion of the electronic structure calculations (below). In support of this, there are many examples (not only the compounds in question) of violations of the Zintl principles in polar intermetallics.[7−9,15,40−41]

Physical Properties. Magnetization (dc mode) as a function of the temperature, obtained in low applied fields during heating and cooling, shows a small peak at around 250 K for $CaMn_2Sb_2$ as seen in Figure 2. This temperature dependence suggests the presence of magnetic spin interactions, which can be attributed to either reorientation of the Mn moments from an initial ferromagnetic to a canted antiferromagnetic state or the occurrence of short-range magnetic order. The variation of the molar susceptibility of $SrMn_2Sb_2$ with the temperature (Figure 2) is comparable and shows a broad hump at around 265 K. The hump temperature gradually becomes lower upon application of a stronger magnetic field. Similar results from dc-magnetization measurements have been previously obtained for $SrMn_2P_2$ and $YbMn_2Sb_2$, which are isostructural with the title compounds.[11,35] In the case of $SrMn_2P_2$, the origin of the magnetic interactions remains unclear even after neutron diffraction studies at various temperatures. In those experiments, the observation of both commensurate and incommensurate superlattice reflections at low temperatures has been interpreted as a consequence of low dimensional long-range magnetic order, which is partially destroyed above some critical temperature.[35a]

Field-dependent dc-magnetization curves for $CaMn_2Sb_2$ obtained at two different temperatures, above and below 250 K, show a relatively steep increase of the magnetization upon increasing the field to $H \approx 5$ kOe, followed by a less steep and almost linear increase with the field and no tendency for saturation (Figure 3). There is virtually no difference between field and zero-field cooling measurements, which indicates that metamagnetic spin-flop transitions are unlikely. The net macroscopic moment on the Mn at 300 K and 50 kOe is only a fraction of a Bohr magneton (ca. 0.15 μ_B/Mn), and evidently, a simple interpretation of its value in terms of localized high/low spin Mn^{2+} ions is unrealistic. The low moment can be viewed as a signature of counterbalancing coupling between Mn atoms that are sitting on two nonequivalent magnetic sites as predicted by theory (below).

To fully understand the magnetism in $CaMn_2Sb_2$ and $SrMn_2Sb_2$, further temperature and field-dependent ac-magnetization measurements were performed on single crystals. These experiments are sensitive probes to detect magnetic phase transitions and can provide information about possible spin reorientation, domain-wall displacements,

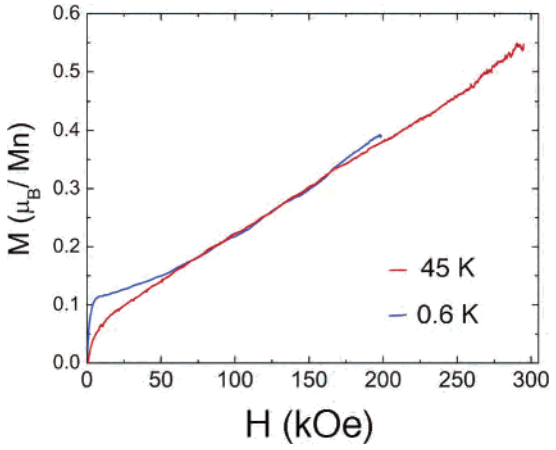

Figure 5. Pulse-field dependence of the ac magnetization for oriented single crystals of $CaMn_2Sb_2$ ($H \parallel c$ axis) at temperatures of 0.6 and 45 K.

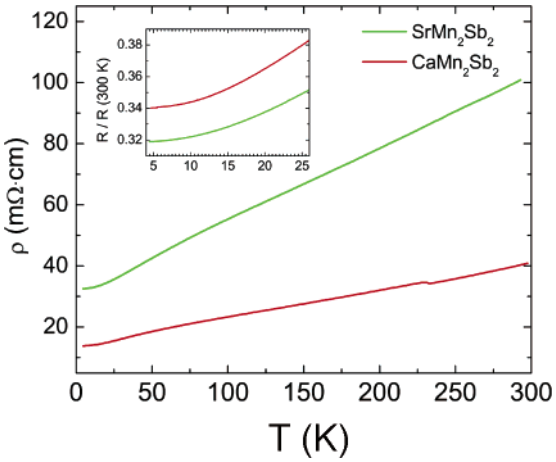

Figure 6. Resistivity as a function of temperature measured on single crystals of $CaMn_2Sb_2$ and $SrMn_2Sb_2$ with the current direction normal to the *ab* plane. Inset shows a magnified view of the plot at low temperature.

magnetic anisotropy, etc. The real component is the "initial" ac susceptibility in phase with the applied ac field, and it is correlated with the reversible initial magnetization process (Figure 4). From these measurements, another transition at ca. 35 K was observed, which vanishes at high fields. The $M-H$ isotherms on oriented single-crystals ($H \parallel c$ axis) taken using a pulsed-field magnet (Figure 5) show behavior very similar to the behavior inferred from the $M-H$ isotherms obtained on an in-house SQUID magnetometer. Again, the data indicate a quick initial increase of the magnetization, followed by an almost linear increase up to very high magnetic fields ($H = 300$ kOe and above) and temperatures as low as 0.6 K. There is neither tendency for saturation nor a sign of a metamagnetic spin-flop transition. A possible conclusion from all bulk magnetic measurements is that the Mn spins form two magnetic sublattices with ferromagnetic coupling within them and strong antiferromagnetic coupling between them. No long-range magnetic order in the direction of the *c* axis is present above 35 K, however, below that temperature and in the presence of low applied fields (below ca. 10 kOe) some short range magnetic order may occur as shown by the anomaly at ca. 35 K in the low ac-field data (Figure 4).

Electrical resistivity measurements as a function of the temperature and field were carried out on single crystals with excitation current applied normal to the *ab* plane. The data (Figure 6) indicate that both $CaMn_2Sb_2$ and $SrMn_2Sb_2$ exhibit metallic-like temperature dependence, although the values of their resistivities at room temperature are significantly higher than those for normal metals: $\rho_{290} = 40$ mΩ cm for $CaMn_2Sb_2$ and $\rho_{290} = 100$ mΩ cm for $SrMn_2Sb_2$. Other components of the resistivity tensor are unavailable as the crystal's morphology did not allow for attaching 4 leads along the direction of the *c* axis. In the temperature range of 5−300 K, the resistivity varies almost linearly with the temperature, and at very low temperatures, it reaches a constant value of $\rho_0 = 13$ mΩ cm for $CaMn_2Sb_2$ and $\rho_0 = 31$ mΩ cm for $SrMn_2Sb_2$. No anomalies in the $\rho(T)$ curves are observed near the temperatures where magnetic transitions were detected in the ac- or dc-susceptibility data. The magnetoresistance defined as $MR = (R_H - R_0)/R_0$ is positive

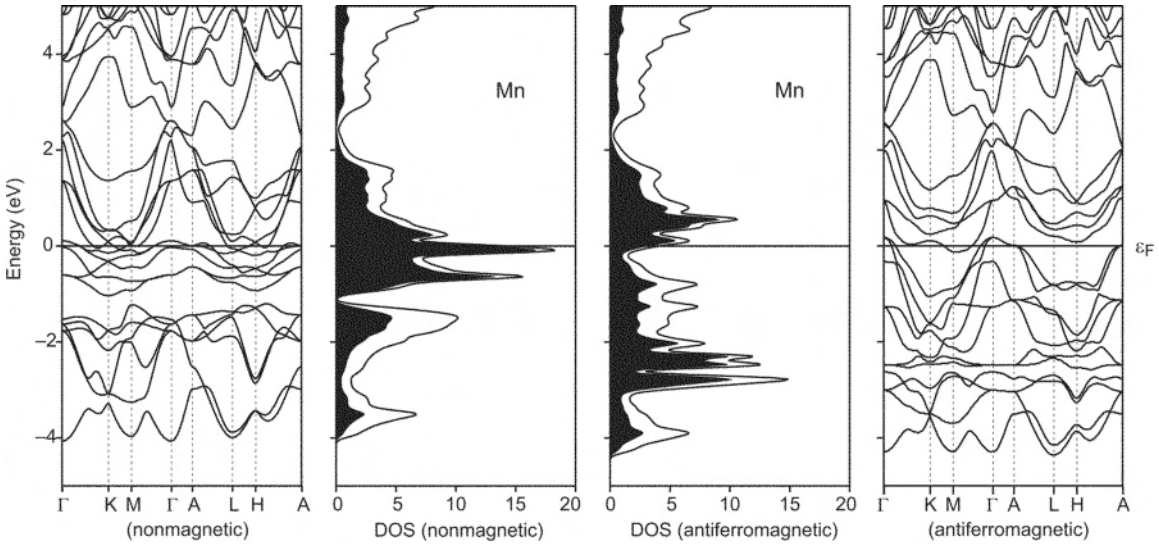

Figure 7. Band structure and total and projected (Mn) DOS in nonmagnetic $CaMn_2Sb_2$, (left), as well as in antiferromagnetic $CaMn_2Sb_2$ (right). The latter structure is characterized by ferromagnetic spin orientations within a single Mn layer and antiferromagnetic spin orientations between two neighboring Mn layers (also see text). All curves are shifted so that the Fermi level (ϵ_F) lies at zero energy.

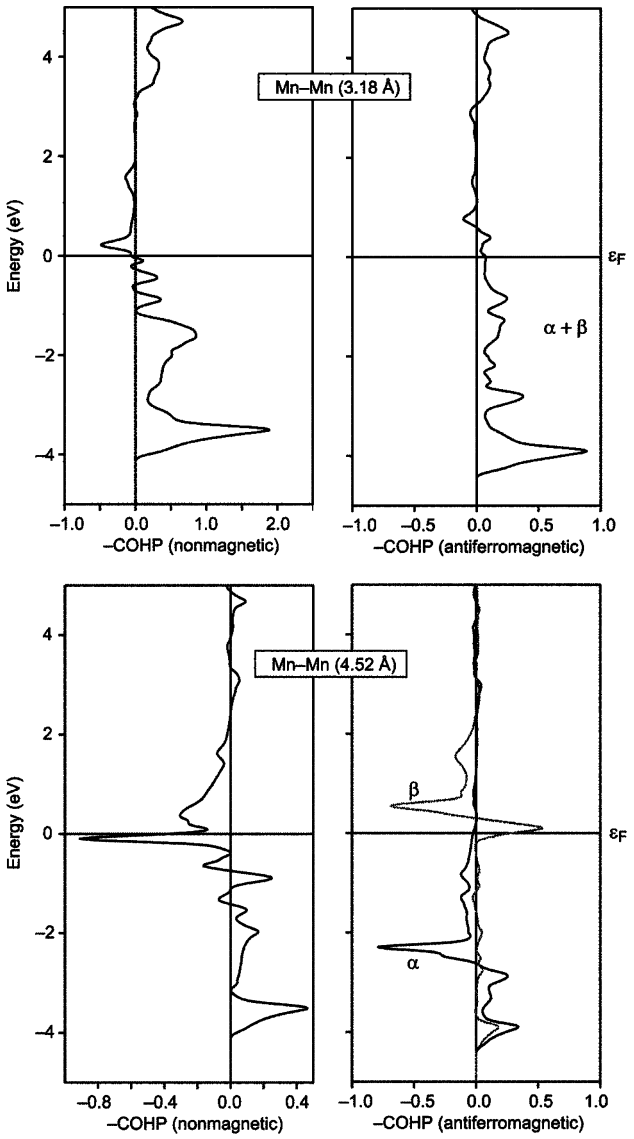

Figure 8. Crystal orbital Hamilton population (COHP) bonding analyses of the nearest (top) and second-nearest (bottom) Mn−Mn interactions in nonmagnetic and antiferromagnetic $CaMn_2Sb_2$ (also see text).

but rather small: it is nonexistent at room temperature and below 1% at 5 K in an applied field of 10 kOe. Such behavior is expected for bulk material with metallic properties and these results are supported by the band-structure calculations.

Electronic Structure. Specific details of the local and extended bonding in $CaAl_2Si_2$-type intermetallics have already been examined by means of the extended Hückel method.[36] Despite being a semiempirical approach which does not allow the proper inclusion of an exchange splitting, a sensible parametrization of the various integrals allows it to provide deep insight into the nonmagnetic part of the bonding forces and at least semiquantitatively explain the electron count and the apparent requirement that the $CaAl_2Si_2$ type is favored over the rival $ThCr_2Si_2$ type for d^0, d^5, and d^{10} configurations.[35,36b] These calculations accurately predict the site preferences and the geometrical distinction between the bonds. However, because these computations do not take spin or magnetic interactions into account, the arguments about whether Mn is in the high- or low-spin d^5-state are difficult to substantiate. Additionally, the extended Hückel calculations in question exclude possible large contributions to the lattice energy from the counterions, which are also likely to have substantial effect on the overall electronic structure. Therefore, to fully understand the unusual magnetic behavior, we carried out spin-polarized DFT calculations on $CaMn_2Sb_2$ as a model.

Table 4. Theoretically (LDA/GGA) Calculated Total and Local Manganese Magnetic Moments (μ_B) and Relative Total Electronic Energies (eV) of the Investigated $CaMn_2Sb_2$ Assuming Nonmagnetic, Ferromagnetic, and Antiferromagnetic Ground States

	k points		μ	μ/Mn	*E*
LDA	756	nonmagnetic	0	0	0
	756	ferromagnetic	6.35	3.19	−1.48
	1500	antiferromagnetic	0	3.35	−2.01
GGA	756	nonmagnetic	0	0	0
	756	ferromagnetic	6.54	3.35	−2.02
	1500	antiferromagnetic	0	3.46	−2.61

The calculated electronic structure and its density of states (DOS) for the nonspin-polarized and spin-polarized (final antiferromagnetic structure) cases are shown in Figure 7. The corresponding analyses of the crystal orbital Hamilton population (COHP) are given in Figure 8. As seen from Figure 7 (left part, nonspin-polarized description), the lowest-lying bands in the band structure consist of manganese s and, mostly, antimony p bands. The bands above them are made up of manganese d levels, which are further mixed with antimony p levels. These bands are isolated from the flat bands near the Fermi level by a gap in the valence region, at about −1 eV. This leads to a sharp spike in the DOS below and exactly at the Fermi level. Let us stick with the nonspin-polarized scenario. In a nonmagnetic world, the Mn−Mn COHPs between the interlayer Mn−Mn contacts (3.178(2) Å, Table 3) are nonbonding at the Fermi level (Figure 8, top left). For a transition metal with a high-exchange splitting, such as Mn, this finding points toward an instability in terms of spin polarization but with *antiferromagnetic* spin orientation, as it is observed in bcc-Cr, for example.[34] On the other hand, the longer (4.52 Å) intralayer Mn−Mn COHPs are strongly antibonding (Figure 8, bottom left), which again suggests spin polarization, but with a *ferromagnetic* spin orientation, just like in bcc-Fe.[34] Thus, both the nearest and second-nearest Mn−Mn bonding interactions point toward a possible energy profit through spin polarization.

Indeed, if the whole structure spin polarizes, the total energy lowers by about 1.5 eV for the LDA and 2 eV for the GGA per unit cell (Table 4). Note that this calculation corresponds to a scenario where are all atomic moments point into the same region of space (a "ferromagnetic" case) such that the new magnetic cell is *identical* to the former crystallographic unit cell. The calculated local magnetic moment on the Mn atom arrives at ca. 3.2 μ_B using LDA and about 3.4 μ_B with GGA; the slightly higher moment for the GGA functional is a typical phenomenon.[34] This is not too far away from earlier neutron diffraction work on $SrMn_2P_2$, which provides evidence for complex magnetic ordering at low temperatures, where the magnetic moment of 4.2 μ_B/Mn has been interpreted as being the high-spin rather than the low-spin state.[35]

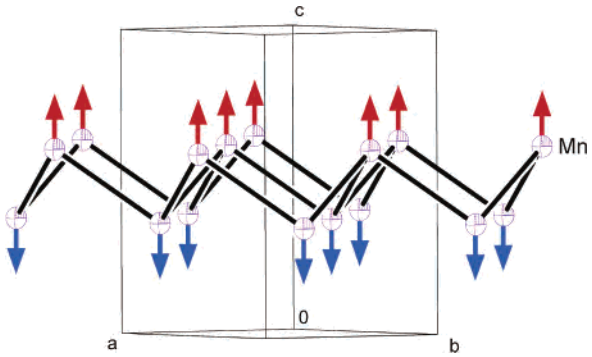

Figure 9. Proposed magnetic structure of $CaMn_2Sb_2$. Mn spins form two parallel magnetic layers with ferromagnetic coupling within them and strong antiferromagnetic coupling between them.

Additional energy stabilization can be achieved if the two Mn sheets are allowed to couple antiferromagnetically as depicted in Figure 9; note that this spin orientation is indicated from the nearest-neighbor Mn−Mn interactions which were nonbonding at the Fermi level. When this model (with a reduced symmetry) is used, DFT calculations indeed show a further energy lowering of about 0.5 eV/unit cell despite the fact that the local magnetic moments on the Mn atom stay almost the same, namely ca. 3.4 μ_B using LDA and 3.5 μ_B using GGA (Table 4). The final result is a structure in which there is ferromagnetic coupling within one Mn sheet (because here Mn−Mn is antibonding) and antiferromagnetic coupling between the sheets (because here Mn−Mn is nonbonding).

The final electronic situation, expressed by an antiferromagnetic cell, is also visible from the band structure (Figure 7, right). Here, the former band gap at about −1 eV has closed because of a downshift of the valence bands near the Fermi region, which has become more disperse. Along the **A** → **L** → **H** → **A** direction, a new gap opens at the Fermi level, but not completely, so that the material remains a metallic conductor. The corresponding spin-resolved COHPs can be seen in the right part of Figure 8. The formerly antibonding Mn−Mn states at the Fermi level have been annihilated because of spin polarization and ferromagnetic spin orientation (Figure 8, bottom) between those Mn atoms, which are 4.52 Å apart. For the Mn−Mn combination at 3.18 Å (Figure 8, top), the formerly nonbonding interactions are not very much affected by spin polarization. Similar phenomena have been found before for the itinerant-magnetic elements of the 3d row. Corresponding calculations have also been carried out for $SrMn_2Sb_2$, and the results (DOS and COHP) very much resemble those of the Ca phase.

Conclusions

The structure and the properties of $CaMn_2Sb_2$ and $SrMn_2Sb_2$ have been studied by means of low-temperature single-crystal X-ray diffraction, temperature and field dependent dc and ac magnetization, field- and temperature-dependent electrical resistivity measurements, and spin-polarized band-structure calculations. The structure and the bonding in these compounds can be rationalized according to the Zintl concept as closed-shell ions requiring a total of 16 valence electrons, an electron count that can be achieved for d^5 and d^{10} transition metals only (e.g., Mn^{2+} and Zn^{2+}). However, despite formally being Zintl phases, both $CaMn_2Sb_2$ and $SrMn_2Sb_2$ are metals, and TB-LMTO calculations confirm a significant contribution of the Mn d bands to the overall bonding, resulting in metallic behavior not associated with delocalized "extra" electrons. Extensive magnetization measurements suggest counterbalancing coupling between Mn atoms that are sitting on two nonequivalent magnetic sites, a hypothesis supported by spin-polarized LDA and GGA DFT calculations, which provides further evidence for a structure in which there is a ferromagnetic coupling within one Mn layer and antiferromagnetic coupling between the layers.[42]

Acknowledgment. S.B. thanks the University of Delaware and the University of Delaware Research Foundation (UDRF) for the financial support of this work. M.G. and R.D. thank the Deutsche Forschungsgemeinschaft (DFG) for financial support. Work at LANL is done under the auspices of U.S. Department of Energy.

Supporting Information Available: An X-ray crystallographic file for the two structures in CIF format. This material is available free of charge via the Internet at http://pubs.acs.org.

IC060092E

(40) Bobev, S.; Bauer, E. D.; Thompson, J. D.; Sarrao, J. L.; Miller, G. J.; Eck, B.; Dronskowski, R. *J. Solid State Chem.* **2004**, *177*, 3545.
(41) Brown, D. E.; Johnson, C. E.; Grandjean, F.; Hermann, R. P.; Kauzlarich, S. M.; Holm, A. P.; Long, G. J. *Inorg. Chem.* **2004**, *43*, 1229.
(42) Note: While this manuscript was under peer-review, another article on the magnetic structure of the structurally related $YbMn_2Sb_2$ appeared (Morozkin, A. V.; Isnard, O.; Henry, P.; Granovsky, S.; Nirmala, R.; Manfrinetti, P. Synthesis and Magnetic Structure of the $YbMn_2Sb_2$ Compound. *J. Alloys Compds.* **2006**, available online Jan 24, http://dx.doi.org/10.1016/j.jallcom.2005.10.051.). The results presented therein are based on neutron diffraction and agree well with the proposed magnetic order in $CaMn_2Sb_2$ and $SrMn_2Sb_2$ (this work).